Detection of Hot Electrons at a p-InP/Pt Rotating Ring/Disk Photoelectrode

Carl A. Koval* and Robert Torres

Contribution from the Department of Chemistry and Biochemistry, University of Colorado, Campus Box 215, Boulder, Colorado 80309

Received March 24, 1993

Abstract: Acetonitrile solutions containing the reversible redox couple decamethylferrocene(1+/0) (DFER, $E^{\circ\prime}$ = –0.40 V) and (dibromoethyl)benzene (DBEB, $E_{1/2}$ = –1.12 V) were used to detect steady-state photocurrent attributable to hot electrons at p-InP photocathodes. Reduction of DBEB at illuminated p-InP disk electrodes produces bromide ions which were quantitatively determined through their oxidation at a Pt ring electrode. Both high-doped and low-doped p-InP electrodes yielded high internal quantum yields for photoconversion (80% and 90%, respectively); however, illumination of high-doped samples invariably produced greater percentages (>30%) of DBEB reduction. Observed dependencies of the percent DBEB reduction on doping density, applied potential, light intensity, and conduction band edge position are all consistent with a type I hot carrier mechanism.

Introduction

Hot-carrier injection of electrons from semiconductor electrodes to solution acceptors utilizes excess excitation energy which is normally lost through thermalization processes. This has the potential to enhance the solar conversion efficiency as well as alter the product distribution in liquid junction solar cells. A solar energy device implementing hot-carrier reactions can convert solar energy with an efficiency of 66%, substantially exceeding the 33% maximum efficiency of a quantum device operating at thermal equilibrium.[1]

Although there is extensive evidence for hot-electron processes in solid-state devices,[2] the evidence for hot-electron reactions in liquid junction cells remains controversial.[3,4] Experimental studies probing hot-carrier effects have been reported by Nozik et al.[5-7] These experiments involved interpretation of current–voltage curves for p-type III–V semiconductors in solutions containing redox couples with reduction potentials negative of the conduction band edge. The first experiment used anthracene as the supra-band-edge redox couple for studies at p-GaP.[5] The second experiment used *p*-nitrobenzonitrile as a probe at p-InP,[6] while the third experiment used tetraethylammonium ions at p-GaP and the production of H_2 at p-InP.[7] Mott–Schottky plots of interfacial capacitance data were used to determine band-edge positions during the experiments. Photocurrent–voltage curves in blank solutions were compared with those of solutions containing the supra-band-edge redox couple. The observation of increased cathodic photocurrent was reported as evidence for hot-electron reductions. Recently, Frese and Chen have postulated hot-electron transport from n-Si(111)/Au to ferricyanide ions in solution to explain a dependence of exchange current density on gold film thickness.[8] Previously, our group has reported hot-electron transfer to solution in a p-InP/acetonitrile photoelectrochemical cell using a copper macrocyclic complex as the redox species in solution.[9] The evidence for hot electrons in this system was the production of copper metal on the surface of the semiconductor. Limitations of this system, which center around alteration of the interface during product formation, have been discussed.[10]

The experimental described herein utilized an illuminated p-InP/Pt rotating ring/disk electrode. The detection scheme for quantifying hot carriers implemented (1,2-dibromoethyl)benzene (DBEB) as the hot-electron acceptor. Upon photoreduction at the p-InP disk, the alkyl halide eliminated bromide anions which could be quantitatively oxidized at the platinum ring to Br_2. The acetonitrile solutions also contained a thermalized electron acceptor, decamethylferrocene (DFER), to prevent movement of the p-InP band-edge positions by accepting electrons at the conduction band edge and not allowing the buildup of charge at the semiconductor surface. The following electrode reactions were found to occur:

Disk/Illuminated p-InP:

$$DFER^+ + e^- \rightleftarrows DFER^0 \qquad \text{(thermalized and hot electrons)}$$

$$DBEB + 2e^- \rightarrow \text{styrene(electro-inactive)} + 2Br^- \qquad \text{(hot electrons only)}$$

Ring/Platinum:

$$DFER^0 \rightleftarrows DFER^+ + e^- \qquad E^{\circ\prime} = -0.40 \text{ V}$$

$$2Br^- \rightleftarrows Br_2 + 2e^- \qquad E^{\circ\prime} = +0.32 \text{ and } +0.67 \text{ V}$$

By modulation of the light and by variation of the potential applied to the ring electrode, it was possible to distinguish the fraction of the photocurrent resulting in reduction of DBEB from the fraction resulting in reduction of $DFER^+$. Results for such experiments performed under a variety of conditions are reported.

Experimental Section

Chemicals and Materials. UV-grade acetonitrile (Burdick–Jackson) was refluxed in CaH_2 under nitrogen for 24 h and distilled. The solvent was then refluxed in P_2O_5 under nitrogen for an additional 24 h and again

(1) Ross, R. T.; Nozik, A. J. *J. Appl. Phys.* **1982**, *53*, 3813.
(2) Reggiani, L. *Topics in Applied Physics. Volume 58. Hot-Electron Transport in Semiconductors*; Springer-Verlag: New York, 1985.
(3) Koval, C. A.; Howard, J. N. *Chem. Rev.* **1992**, *92*, 411–433.
(4) Lewis, N. S. *Annu. Rev. Phys. Chem.* **1991**, *42*, 543–579.
(5) Turner, J. A.; Nozik, A. J. *Appl. Phys. Lett.* **1982**, *41*, 101.
(6) Nozik, A. J.; Cooper, G.; Turner, J. A.; Parkinson, B. A. *J. Appl. Phys.* **1983**, *54* (11), 6463.
(7) Nozik, A. J.; Thacker, B.; Turner, J. A. Hot Carrier Effects at the Semiconductor Electrolyte Interface. *Proceedings of Electrodynamics and Quantum Phenomena at Interfaces*; Georgian Academy of Sciences: Telavi, Georgia, USSR, 1984.
(8) Frese, K. W., Jr.; Chen, C. *J. Electrochem. Soc.* **1992**, *139* (11), 3243.
(9) Koval, C. A.; Segar, P. R. *J. Am. Chem. Soc.* **1989**, *111*, 2004.
(10) Koval, C. A.; Segar, P. R. *J. Phys. Chem.* **1990**, *94* (5), 2033.

0002-7863/93/1515-8368$04.00/0

distilled. The doubly distilled acetonitrile was then transferred immediately to a helium-filled drybox (Vacuum Atmospheres). Tetrabutylammonium fluoroborate (TBAFB) (Southwestern Analytical) was recrystallized twice from absolute ethanol and dried under vacuum for 5–7 days. All solutions were 0.1 M in TBAFB. (1,2-Dibromoethyl)benzene (DBEB) (Aldrich Chemicals) was recrystallized twice from diethyl ether. Bis(pentamethylcyclopentadienyl)iron, more commonly referred to as decamethylferrocene (DFER) (Strem Chemicals), was purified by sublimation. Solutions containing DFER were electrolyzed at constant potential to a Nernst ratio of approximately 90:10 oxidized/reduced.

Single-crystal InP wafers were obtained with (100) orientation from Crystacomm Inc. n-Type InP was doped with tin, while p-type InP was doped with zinc. Different crystal numbers refer to wafers obtained from different ingots. Crystal number 4122 was zinc doped at a density of 1.23×10^{18} cm^{-3} (as reported from the manufacturer), with a thickness of 625 μm. Crystal number 2720 was also zinc doped but at a density of 3.56×10^{18} cm^{-3}, with a thickness of 600 μm. Crystal number 3189 was zinc doped at a density of 8.0×10^{15} cm^{-3}, with a thickness of 625 μm. Crystal number 3239 was tin doped at a density of 1.5×10^{18} cm^{-3}, with a thickness of 625 μm. For simplification, a doping density of 10^{18} cm^{-3} is referred to as high doped, while one of 10^{15} cm^{-3} is referred as low doped.

Electrode Preparation. The platinum ring electrode was prepared using a Buehler Ltd. polisher, sequentially polishing with 5-, 1-, 0.3-, and 0.05-μm alumina particles. The electrode was then sonicated in water to remove excess alumina and dried. The reference electrode consisted of a silver wire placed in a 0.01 M $AgNO_3$ solution encapsulated in a small glass tube with a 4-mm Vycor frit (Princeton Applied Research). All potentials are reported vs this reference electrode.

A rotating ring/removable disk electrode (RRDE) was purchased from Pine Instrument Co., Model AFDTI-36 PTPTT. The removable platinum disk assembly was detached from the body of the electrode and duplicated with the InP semiconductor substituting for the platinum metal. The disk assembly consisted of a brass shaft which screws into the body of the electrode making the necessary electrical contact. The head of the disk assembly is machined so that a secure friction fit is obtained between the outer circumference of the brass shaft and the inner circumference of the Teflon u-cup. Fabrication of the semiconductor disk assembly consisted of machining the brass shaft with the appropriate screw threads. Since epoxy was applied over the brass for electrical insulation, the diameter of the brass mount was machined smaller than usual to ensure a secure fit when placed in the Teflon u-cup. Zinc powder was fused onto the back of the p-Inp wafer, while tin powder was fused onto the back of the n-InP wafer. The InP wafer was then cut into a square pattern which encompassed the entire face surface area of the brass mount assembly. An Ohmic contact was made from the InP wafer to the brass mount assembly by first applying InGa–amalgam to the back of the semiconductor (over the fused material) and then cementing the wafer to the brass assembly using conductive silver epoxy, Model Number H20E (Epoxy Technology Inc.). Once the epoxy hardened, the electrode was carefully wet hand sanded with fine-grit silicon carbide abrasive paper until a semicircular shape was obtained. The electrode was then placed in a lathe and rotated at a very slow speed while being wet sanded. This procedure continued until the InP disk was the same diameter as the brass mount assembly. Hysol Epoxy-Patch 56C, used as an insulator, was then applied to the brass and the circumference of the InP. The utmost precautions were taken to completely cover the edge sites of the InP while not placing the insulating epoxy on the surface of the InP. The white insulating epoxy was allowed to dry and was then sanded to a diameter which securely fit into the Teflon u-cup. Throughout the entire fabrication procedure of the semiconductor RRDE, the surface of the InP wafer was never abraded. The shaping, epoxy application, and epoxy removal from the electrode had no visible effect on the surface of the InP wafer. The InP removable disk electrode (RDE) was then chemomechanically etched in a Br_2/methanol solution, as described previously.[9] The resulting InP surfaces were smooth and mirror-like, with surface areas near 0.16 cm^2.

Photoelectrochemical experimental procedures have been described previously.[9]

Results

Electrochemistry of (1,2-Dibromoethyl)benzene at Platinum Electrodes. Two sequential cyclic voltammetric (CV) scans of 3 mM DBEB at platinum are shown in Figure 1. The potential

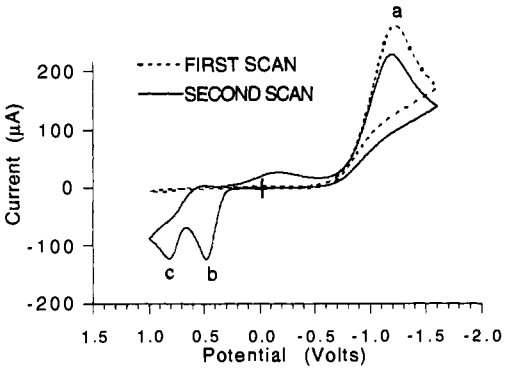

Figure 1. Cyclic voltammograms of 3 mM DBEB at platinum Scan rate was 500 mV/s.

scan begins at 0.0 V, starts positive to +1.0 V, reverses direction to −1.7 V, returns to 0.0 V, and repeats. In the negative portion of the scans, an irreversible wave (a) due to the reduction of DBEB is observed. The peak current for the second scan is diminished because a fraction of the DBEB is removed from the diffusion layer. In the first scan, the lack of anodic current is apparent. In the second scan, bromide created in the reduction of DBEB is oxidized with peak potentials of +0.43 V (wave b, Figure 1) and +0.73 V (wave c, Figure 1). The electrochemistry of $Br_2/Br^-/Br_3^-$ has been studied and characterized by Marchon et al.[11] Waves b and c and their accompanying reduction peaks are consistent with this earlier work.

On the basis of cyclic voltammograms, there appears to be no other electroactive species generated during the reduction of DBEB. To confirm this result, a bulk electrolysis of 7.8 mM DBEB was performed with a platinum gauze electrode at −1.4 V. After the electrolysis, 23.23 C of charge had passed, resulting in an *n*-value of 2.05. Using the method of standard addition and measuring peak currents for Br^- oxidation, the Br^- concentration was calculated to be 15.4 mM. On the basis of the initial concentration of DBEB, if a single bromine was reductively eliminated, the theoretical bromide concentration would equal 7.83 mM. If both bromides were reductively eliminated, the theoretical bromide concentration would equal 15.6 mM. Cyclic voltammograms obtained before and after the bulk electrolysis revealed the only electroactive species present after the bulk electrolysis was the $Br^-/Br_3^-/Br_2$ couple. Styrene (5 mM) was then added; the addition of styrene had no effect on the shape of the cyclic voltammogram, indicating styrene is not electroactive in the potential window of interest. Furthermore, gas chromatographic analysis revealed the product of the bulk electrolysis to be styrene. The concentration of styrene was determined to be equal to the initial concentration of DBEB.

Electrochemistry of DBEB at n-InP. A critical part of this experiment was determining where the reduction of DBEB took place relative to the conduction band edge of the p-InP semiconductor. This was approximated by investigating the reduction of DBEB at n-InP electrodes in the dark at negative potentials where n-InP entered accumulation. In this condition, the semiconductor can supply a sufficient amount of electrons to the surface such that the behavior is similar to that of a metal electrode. This behavior is not attainable at a p-InP electrode in the dark but is a good approximation for the reduction potential of DBEB at p-InP, since the conduction band energies (E_{CB}) for the two materials are similar.[12,13] Factors which may cause discrepancies in the reduction potentials of equally doped p-InP and n-InP

(11) (a) Parsons, R. *Handbook of Electrochemical Constants*; Butterworths: London, 1959; p 73. (b) Strehlow, H. Z. *Elektrochem.* **1952**, *56*, 827. (c) Kortum, G. *Treatise on Electrochemistry*, 2nd rev. Engl. ed.; Elsevier: Amsterdam, The Netherlands, 1965; p 312. (d) Marchon, J. C. *C. R. Acad. Sci. Paris, Ser. C* **1968**, *267*, 1123.

(12) Koval, C. A.; Austermann, R. L. *J. Electrochem. Soc.* **1985**, *132* (11), 2656.

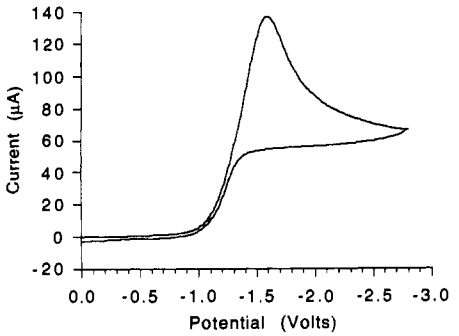

Figure 2. Cyclic voltammogram of 2 mM DBEB at high-doped n-InP. The scan rate was 100 mV/s.

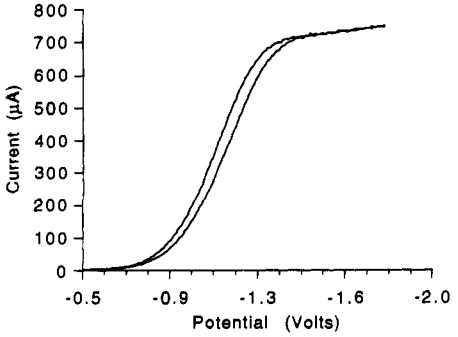

Figure 3. Rotated voltammogram of 2 mM DBEB at high-doped n-InP at a rotation rate of 1000 rpm. The scan rate was 5 mV/s.

electrodes are due to intrinsic differences in the dopant. Also, the resistivities and etch pit densities of n- and p-type materials both differ by approximately 1 order of magnitude.

A cyclic voltammogram of 2 mM DBEB at high-doped n-InP is shown in Figure 2 at a scan rate of 100 mV/s. The peak current for the irreversible wave occurred at a potential of −1.58 V. A rotated voltammogram of 2 mM DBEB at 1000 rpm is shown in Figure 3 at a scan rate of 5 mV/s. The $E_{1/2}$ in the rotated voltammogram occurred at −1.12 V.

Electrochemistry of DBEB at Rotated p-InP Disk Electrodes. Figure 4 contains dark and light current–voltage curves obtained at p-InP under solution conditions identical to those of the subsequent RRDE light modulation experiments. This data corresponds to data sets c and e in Tables I and II, respectively. The results for the high-doped p-InP electrode revealed the photocurrent onset potential to be near −200 mV. The cathodic dark current increases as the potential is biased negative. This dark "leakage" current is due to the relatively high concentration of dopant atoms present in the semiconductor. The observed current–voltage curve displays typical behavior for a highly doped p-InP electrode.[12] The illuminated scan parallels the dark scan while sustaining a photocurrent of approximately 27 μA over the dark current. The low-doped electrode exhibited zero dark current from −400 to −1200 mV with the photocurrent onset potential near −200 mV. The low-doped sample exhibited a higher light-limited photocurrent of 35 μA.

Detection of Hot Carriers Using a p-InP/Pt RRDE. As discussed below, the conduction band edge for p-InP in acetonitrile solutions containing 0.5 M $DFER^{+,0}$ (90:10) and 10 mM DBEB is −1.2 ± 0.1 V. Photogenerated electrons that thermalized to E_{CB} will reduce $DFER^+$ at a mass transport limited rate. Assuming that the kinetics for reduction of DBEB at n- and p-InP are similar, electrons at −1.2 V will also be capable of reducing DBEB at a kinetically controlled rate. The products of these reduction processes will be swept past the Pt ring.

(13) (a) Bard, A. J.; Fan, F. F.; Wheeler, B. L.; Nagasubramanian, G. *J. Electrochem. Soc.* **1982**, *129*, 1742. (b) Koval, C. A.; Segar, P. R.; Koel, B.; Gebhard, S. *J. Electrochem. Soc.* **1990**, *137* (2), 544.

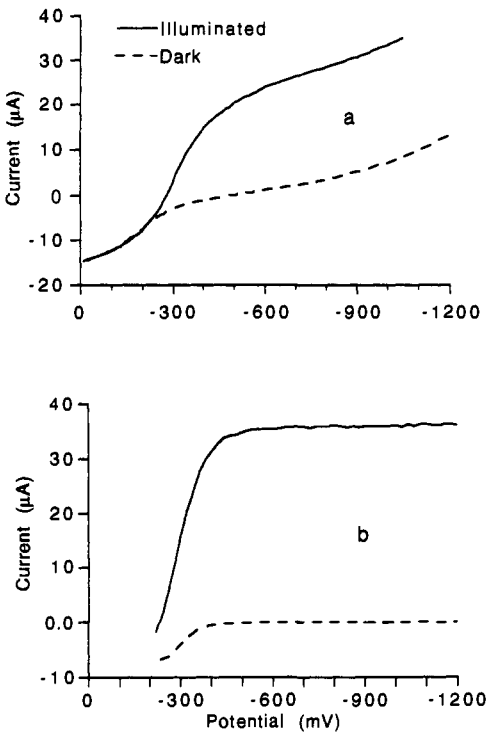

Figure 4. Rotated voltammograms for high-doped (a) and low-doped (b) illuminated p-InP electrodes in 0.5 mM $DFER^{+/0}$ (90:10) and 10 mM DBEB under 0.43 mW/cm² illumination at 543.5 nm. The scan rate was 25 mV/s.

Table I. RRDE Light Modulation Data for High-doped p-InP, 0.5 mM $DFER^{+/0}$ (90:10), 10 mM DBEB, 1000 rpm, 543.5 nm

expt[a]	applied potential (V)	disk photocurrent[b] (μA)	ring response to disk photocurrent (μA) E_R = +0.2 V[b]	ring response to disk photocurrent (μA) E_R = +0.8 V[b]	$-I_R/I_D$	percent hot photocurrent[c]
a	−1.0	44.0 ± 0.4	6.5 ± 0.2	9.65 ± 0.2	0.22	33 ± 2
a	−0.8	44.5 ± 0.4	7.6 ± 0.2	10.0 ± 0.2	0.22	25 ± 2
a	−0.6	37.5 ± 0.4	7.2 ± 0.2	8.0 ± 0.2	0.21	10 ± 3
b	−1.0	43.5 ± 0.5	5.8 ± 0.1	8.8 ± 0.1	0.20	35 ± 2
b	−0.8	36.5 ± 0.5	5.9 ± 0.1	7.5 ± 0.1	0.20	22 ± 2
b	−0.6	30.0 ± 0.5	5.7 ± 0.1	6.2 ± 0.1	0.21	8 ± 2
c	−1.0	23.5 ± 0.4	3.9 ± 0.1	4.3 ± 0.1	0.18	9 ± 3
c	−0.8	24.0 ± 0.4	4.0 ± 0.1	4.3 ± 0.1	0.18	6 ± 3
c	−0.6	20.0 ± 0.4	3.5 ± 0.1	3.6 ± 0.1	0.18	0

[a] E_{CB} = −1.20 V, crystal no. 4122 (expt a); E_{CB} = −1.21 V, crystal no. 4122 (expt b); E_{CB} = −1.18 V, crystal no. 4122, photon flux attenuated by 50% (expt c). [b] Averaged value from several data points. [c] Defined in text.

Table II. RRDE Light Modulation Data for Low-Doped p-InP, 0.5 mM $DFER^{+/0}$ (90:10), 10 mM DBEB, 1000 rpm, 543.5 nm

expt[a]	applied potential (V)	disk photocurrent[a] (μA)	ring response to disk photocurrent (μA) E_R = +0.2 V[a]	ring response to disk photocurrent (μA) E_R = +0.8 V[a]	$-I_R/I_D$	percent hot photocurrent[c]
d	−1.0	52.0 ± 0.4	9.8 ± 0.2	11.0 ± 0.2	0.21	11 ± 2
d	−0.8	50.5 ± 0.4	9.6 ± 0.2	10.7 ± 0.2	0.21	10 ± 2
d	−0.6	49.5 ± 0.4	9.1 ± 0.2	9.4 ± 0.2	0.19	3 ± 2
e	−1.0	27.5 ± 0.4	6.0 ± 0.1	6.1 ± 0.1	0.22	0
e	−0.8	27.5 ± 0.4	5.9 ± 0.1	6.1 ± 0.1	0.22	0
e	−0.6	27.5 ± 0.4	6.2 ± 0.1	6.3 ± 0.1	0.23	0

[a] E_{CB} = −1.24 V, crystal no. 3189 (expt d); E_{CB} = −0.99 V, crystal no. 3189, photon flux attenuated by 50% (expt e). [b] Averaged value from several data points. [c] Defined in text.

Reduction of $DFER^+$ can be detected at the Pt ring if its potential is held positive of ca. −0.3 V. Reduction of DBEB can be sensed at the Pt ring by holding the potential sufficiently positive to

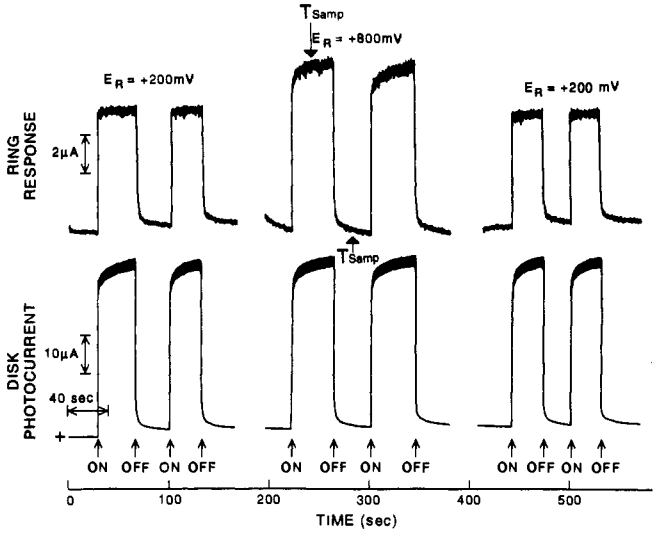

Figure 5. Platinum ring (top) and high-doped p-InP disk (bottom) raw data corresponding to data b in Table I. Zero ring current is off scale at this attenuation and therefore is not shown. T_{samp} represents measuring a data point at a designated time after the light source was illuminated or darkened. Experimental conditions included 0.5 mM $DFER^{+/0}$ (90:10), 10.4 mM DBEB, 1000 rpm, under 0.84 mW/cm^2 illumination at 543.5 nm. The disk potential was −1.0 V.

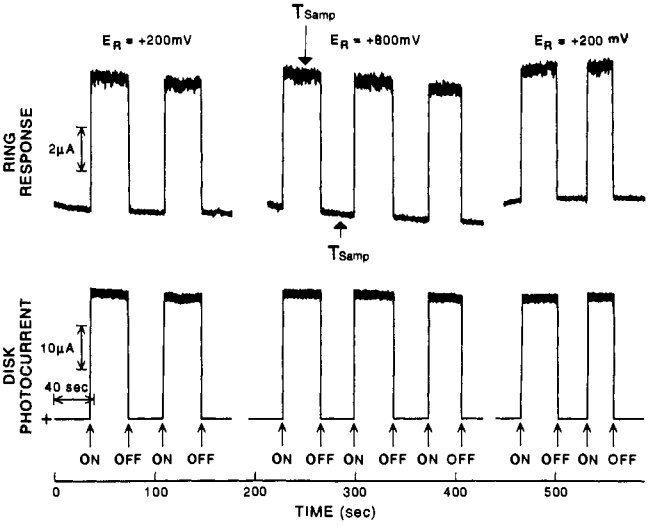

Figure 6. Platinum ring (top) and low-doped p-InP disk (bottom) raw data corresponding to data e in Table II. Zero ring current is off scale at this attenuation and therefore is not shown. T_{samp} represents measuring a data point at a designated time after the light source was illuminated or darkened. Experimental conditions included 0.5 mM $DFER^{+/0}$ (90:10), 10.4 mM DBEB, 1000 rpm, under 0.43 mW/cm^2 illumination at 543.5 nm. The disk potential was −1.0 V.

oxidize Br^- to Br_2, i.e. ca. +0.8 V. At these more positive potentials, DFER will also be oxidized, but the portion of the ring current due to oxidation of DFER can be determined independently, i.e. at potentials between −0.3 and +0.2 V. Therefore the difference in the ring current at +0.2 V (where oxidation of DFER is occurring but no oxidation of Br^- is occurring) and +0.8 V (where oxidation of DFER is occurring and oxidation of Br^- to Br_2 is occurring at a mass transport limiting rate) can be attributed solely to bromide oxidation.

In order to determine the fraction of photocurrent resulting in reduction of DBEB, rotating p-InP/Pt RRDE's were illuminated periodically with defocused laser light. The laser was defocused such that the area of the beam was several times larger than the electrode area, causing the intensity to vary by ≈30% from the edge of the electrode to the center. Cathodic currents were recorded for the disk and anodic currents for the ring. Typically, collection efficiencies ($-i_R/i_D$) approached the theoretical value of 20% ± 2% between experiments and varied by <1% during any given experiment (see Tables I and II). The variation of the actual collection efficiency relative to the theoretical value resulted from the dissimilar placement, from one experiment to another, of the p-InP disk in the disk housing assembly.

Experiments were performed on both high- and low-doped p-InP photocathodes under different degrees of band bending and light intensity. Typical raw data for these experiments are contained in Figures 5 and 6. As mentioned earlier, when the platinum ring was set at +0.2 V, anodic current was due solely to oxidation of DFER. When the platinum ring was set to +0.8 V, the anodic current was due to oxidation of DFER and Br^-. Therefore the difference in ring current at +0.2 and +0.8 V was attributed to bromide oxidation. A typical experiment began by biasing the darkened p-InP disk near the photocurrent onset potential and observing the current response at both the ring (E_R = +0.2 V) and disk electrodes. The p-InP disk was illuminated for approximately 30 s and again darkened for approximately 30 s. This was repeated through several cycles. During the last cycle in the dark, the platinum ring potential was adjusted to +0.8 V and the illumination/dark cycles were repeated. After several cycles of data had been obtained, the potential of the platinum ring was re-adjusted to +0.2 V during the dark portion of the cycle. Once again the illumination/dark cycles were repeated several times. The potential applied to the InP disk was then adjusted negative by increments of −0.2 V, and the entire process was repeated. The negative bias on the InP disk was increased to approximately −1.0 V. This results in the maximum amount of band bending and the greatest magnitude in electric field in the space charge region (SCR) without causing the interface to become inverted.

Capacitance Measurements. Determination of the band-edge positions of the p-InP electrode is extremely important in the analysis and interpretation of the rotating ring/disk experiments. We have shown previously that the band-edge positions of p-InP shift with solution potential, indicating the occurrence of Fermi level pinning.[13b] It was found that the flat band potential shifts linearly with the potential of the redox couple present in solution with a slope of ca. 0.55. Gorochov et al. have reported similar effects at n-GaAs placed in acetonitrile containing different redox reagents.[14] Fermi level pinning was also reported by Bard et al. at p-Si in acetonitrile solutions containing different redox couples.[13a] The conditions required for the observation of stable interfacial energetics during photoelectrochemical experiments for p-InP/CH_3CN have been discussed in several previous publications.[9,10,13b,16,17] Shifts in the band-edge position were avoided in the experiments reported herein by the presence of the poised $DFER^{+,0}$ couple. Additionally, the solution potential is nearly the same when the electrode is in the dark and under illumination because the light intensities used are relatively low and because the solution is stirred.

Capacitance vs potential data were obtained before and after the ring/disk experiments in the dark and under illumination using the exact same conditions of rotation rate, light intensity, concentration, and potential range. A typical Mott–Schottky (M–S) plot ($1/C_{sc}^2$ vs E_D) derived from these data is contained in Figure 7. These data were obtained before and after a ring/disk experiment under illumination. M–S plots obtained in the dark and under two different light intensities are shown in Figure 8. The band-edge positions did not shift within experimental

(14) Gorochov, O.; Fotouhi, B.; Gabouze, N.; Cachet, H.; Yao, N. A. *J. Electroanal. Chem.* **1987**, *237*, 289.

(15) (a) SZE, S. M. *Physics of Semiconductor Devices*; Wiley-Interscience: New York, 1981. (b) Gerischer, H. *Physical Chemistry: An Advanced Treatise*; Eyring, H., Ed.; Academic: New York, 1970; Vol. 9, pp 463–542.

(16) Koval, C. A.; Segar, P. R. *J. Electrochem. Soc.* **1988**, *135* (10), 2655.

(17) Koval, C. A.; Austermann, R. L.; Turner, J. A.; Parkinson, B. A. *J. Electrochem. Soc.* **1985**, *132* (3), 613.

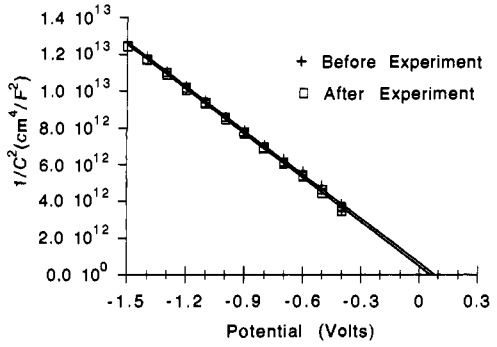

Figure 7. Mott–Schottky plots for high-doped p-InP in 0.5 mM $DFER^{+/0}$ (90:10) and 10 mM DBEB acquired immediately preceding and directly following the RRDE light modulation experiments under 0.84 mW/cm^2 illumination at 543.5 nm at 5000 Hz. These data include the forward and reverse scans.

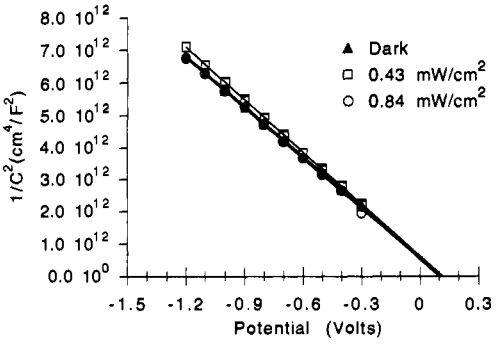

Figure 8. Mott–Schottky plots for high-doped p-InP in 0.5 mM $DFER^{+/0}$ (90:10) and 10 mM DBEB acquired immediately preceding the RRDE light modulation experiments under various illumination conditions at 543.5 nm at 5000 Hz. The data includes the forward and reverse scans. The band-edge positions are determined from the x-intercept.

error in all cases. In a separate experiment, the band-edge positions were monitored in the presence of 0.5 mM $DFER^{+,0}$ only. DBEB was then added to make the resulting solution 10 mM DBEB and 0.5 mM $DFER^{+,0}$. The addition of DBEB had no effect on the band-edge positions.

It is essential that the M–S plots exhibit no frequency dispersion, as it is well-known that the frequency dependence is indicative of nonideal behavior[15] and results in unreliable measurements of flat band potentials. The frequency dependence was measured from 500 to 10 000 Hz under conditions identical to those of the ring/disk light modulation experiments. Once again the flatband potential did not shift within experimental error. All M–S plots reported herein were obtained at 5000 Hz. Doping densities derived from M–S plot slopes agreed with those provided by the manufacturer to within 50%. This provides further evidence for the validity of the band-edge positions measured by this method. In general, all M–S plots were nonhysteretic, linear, frequency independent, and reproducible. The high degree of linearity observed in the M–S plots implies the band edges remain stable over the potential range that the space charge capacitance values were measured. Relevant equations and procedures for determination of band-edge positions from these plots have been described previously.[9] Values of E_{CB} for the p-InP disk are given for every experiment reported in Tables I and II.

Summary of Results. Portions of the data for five Pt/ring p-InP/disk experiments are summarized in Tables I and II. Table I contains data for three separate experiments labeled a, b, and c, each utilizing high-doped p-InP at three common disk potentials. Table II contains similar data for two experiments labeled d and e utilizing low-doped p-InP. The uncertainties associated with the values in Tables I and II were obtained by measuring the peak to peak noise and dividing by 5. These uncertainties were propagated in the collection efficiency and percentage of hot photocurrent calculations. The percentage of the disk photocurrent resulting in reduction of DBEB, which is referred to as the hot photocurrent, was calculated by dividing the difference of the ring current at +0.2 and +0.8 V by the ring current at +0.8 V and multiplying by 100.

The data in Table I for high-doped samples reveals that a significant fraction (up to 35%) of the disk photocurrent results in reduction of DBEB. The experiments represented by lines a and b in Table I are under nearly identical conditions except that they were performed a month apart. Experiment c was performed with the same electrode and solution conditions as b; however, a neutral density filter was placed in the path of the illumination source, which attenuated the photon flux by 0.5. Each of the three experiments in Table I reveals a strong dependence of the percent hot photocurrent on the applied potential. The position of the conduction band edge (E_{CB}) is given for each experiment. As explained above, the capacitance vs potential data used to obtain these values were recorded using the same solution conditions and applied potentials as those used for the data in the tables. These measurements indicated that the position of E_{CB} was not changing with applied potential.

The data for low-doped p-InP electrodes are presented in Table II. The lines representing experiment d are for a light intensity similar to that for experiments a and b in Table I. The position of E_{CB} for this experiment is similar to the values for the experiments in Table I; however, a significantly lower percentage of DBEB reduction relative to that for the high-doped material is observed. Experiment e was obtained with the photon flux attenuated as in experiment c in Table I. Experiment e also utilized a different p-InP electrode, and the value of E_{CB} is approximately +200 mV with respect to those for the other four experiments. These data revealed the absence of any DBEB reduction.

Experiment e provides the rationale for referring to the percentage of the disk photocurrent resulting in reduction of DBEB as the hot photocurrent. As shown in the voltammogram for a rotating n-InP electrode in Figure 3, reduction of DBEB begins to occur at about –0.7 V. For the low-doped electrode used in experiment e, photogenerated electrons arriving at the interface, presumably with an energy equivalent to E_{CB}, react exclusively with $DFER^+$, which has a redox energy within the band gap of p-InP. Reduction of DBEB only occurs when E_{CB} approached –1.2 V and becomes substantial only with highly doped p-InP. In these situations, some fractions of the photogenerated electrons appear to have enhanced reducing capacity.

The experiments summarized in Tables I and II are representative of data obtained for other electrodes where photoreduction of DBEB is observed. The disk photocurrents tend to plateau near E_D = –0.8 V, indicating that further band bending does not increase the efficiency of charge separation. Since the collection efficiency for a given RRDE does not change during an experiment, the overall ring response to disk photocurrent ($i_R^{+0.8}/i_D$) remains constant with applied potential. However, the ratio of ring current (due to DFER) to disk photocurrent ($i_R^{+0.2}/i_D$) diminishes with increased band bending, indicating a greater rate of reduction of DBEB. At comparable potentials and light intensities, high-doped samples produced significantly more hot photocurrent than low-doped samples. Decreasing the light intensity leads to a reduction in the percent hot photocurrent for both high-doped and low-doped samples.

Although the etching solution and procedure is nominally identical for all electrodes, the electrochemical behavior of these electrodes can be drastically different. For any electrode, it is possible to observe no hot photocurrent. X-ray photoelectron spectroscopy experiments are currently underway to determine if there is a difference in the composition of the surfaces of the electrodes that produce hot photocurrent and those electrodes

that produce little or no hot photocurrent. Typically an electrode which does not produce hot photocurrent can be induced to generate hot photocurrent by repeating the etching procedure one or more times. Although one can ultimately induce hot photocurrent in any given electrode, the percentage of hot photocurrent can vary extensively from one electrode to another.

Quantum Yields/Other Redox Couples. The experiments summarized in Tables I and II utilized two light intensities. The photon flux was measured to be 0.84 mW/cm^2 without the neutral density filter, and 0.43 mW/cm^2 when attenuated with the neutral density filter. Theoretical photocurrents were calculated for these two intensities using the measured laser output and correcting for reflection and other optical losses.[9] The theoretical photocurrent was 59 ± 6 μA without the use of the neutral density filter. Total disk photocurrents for the high-doped electrode at E_D = −1.0 V were approximately 44 μA, resulting in an internal quantum yield of 75%. The low-doped electrode sustained a photocurrent of 52 μA at E_D = −1.0 V, resulting in an internal quantum yield of 88%. Use of the neutral density filter to produce a lower light intensity did not significantly affect the quantum yield values. The theoretical photocurrent was calculated to be 30 ± 3 μA when the neutral density filter was implemented. Total disk photocurrents for the high-doped electrode at E_D = −1.0 V were approximately 24 μA, resulting in an internal quantum yield of 80%. The low-doped electrode sustained a photocurrent of 27 μA at E_D = −1.0 V, resulting in an internal quantum yield of 90%. Incomplete absorption of the light in the depletion region as well as recombination of the photogenerated electrons and holes in the bulk and at surface states is thought to limit the quantum yields. A higher quantum yield was observed for the low-doped electrode as a result of more photons being absorbed in the wider space charge region.

The reversible redox couple used in these experiments, DFER$^{+\cdot,0}$, serves two purposes. First, the presence of DFER$^+$ is necessary in order to remove thermalized photogenerated electrons from the electrode surface, which prevents band-edge movement under illumination. Second, the solution potential established by the poised DFER$^{+\cdot,0}$ couple determined the p-InP/CH_3CN interfacial energetics, i.e. the position of E_{CB}.[13,14] By using different reversible couples, it should be possible to alter the fraction of photocurrent resulting in reduction of DBEB.

Attempts to use couples with reduction potentials negative of that of DFER$^{+\cdot,0}$, specifically 1,1′-diphenylphosphinocobaltocene(1+/0), 1,1′-dicarbomethoxycobaltocene(1+/0), and cobaltocene(1+/0), were unsuccessful because the reduced forms of these couples were found to be unstable in the presence of DBEB. It was possible to use couples, such as ferrocene(1+/0), with $E^{\circ\prime}$ positive of that of DFER$^{+\cdot,0}$. Use of ferrocene(1+/0) to poise the solution potential resulted in a +350-mV shift of E_{CB} for the p-InP disk. The results of the ring/disk experiments using ferrocene(1+/0) revealed no DBEB reduction under all previously described experimental conditions.

Discussion

Comparison to Previous Research. Previous research by our group on the photoreduction of Cu(II,I,0)trans-diene(2+/1+/0) at p-InP/CH_3CN led to the conclusion that for high-doped electrodes a significant fraction of the photogenerated electrons were injected into the solution at energies negative of the conduction band edge.[9] The results reported here for the DFER$^{+\cdot,0}$/DBEB redox system are in complete agreement with those for the Cu-system even though the molecules involved and the measurement techniques are entirely different. In the Cu-system, the product of the hot-electron reaction (Cu metal) was insoluble in the electrolyte and was detected by its deposition on the electrode surface. In contrast, reduction of DBEB produces soluble and stable products (styrene and bromide ion) that can be detected at a second electrode. One marked advantage of this type of redox system for investigating hot-electron processes is that the p-InP electrode is not altered during the experiment; therefore, currents remain temporally stable. The results for the DBEB system are also more convincing and potentially more useful for answering remaining mechanistic questions about this process, because the effect is observable at both high- and low-doped samples.

A second important advantage of the DBEB/metallocene system is the ability to independently vary the concentrations of the thermalized electron (metallocene) and hot-electron (DBEB) acceptors. It is also possible to "tune" the value of E_{CB} by using metallocenes with different reduction potentials. As demonstrated by Segar et al.,[13] E_{CB} for p-InP varies by about 60 mV for a 100-mV change in the solution potential. By poising the solution with ferrocene(FER)(1+/0) as opposed to DFER$^{+\cdot,0}$, E_{CB} shifts positive by approximately 300 mV to nearly −0.9 V. Under these conditions, photogenerated minority carriers created at either high- or low-doped p-InP exclusively reduced FER$^+$, i.e. reduction of DBEB to produce bromide ions is not observed. This result confirms the conclusion, reached in both the Cu(trans-diene) and present study, that the hot photoelectrons observed at high-doped p-InP are only 200 to 300 mV hot with respect to E_{CB}.

In the experiments reported in this paper, it was necessary to bias the p-InP electrodes negative of the solution potential in order to achieve the large amount of band bending required for observation of hot electrons. This means that the cell was not storing energy when the hot photoreaction was being observed. For this reason, it would be interesting to use thermal electron acceptors with reduction potentials negative of DFER$^{+\cdot,0}$. Unfortunately, so far, attempts to perform such experiments have been thwarted by the fact that very reducing couples, such as cobaltocenes, react homogeneously with DBEB. It should be noted, however, that in the case of the Cu(trans-diene) system hot-electron photoproducts were observed at applied potentials where the photoreaction involving the thermal electron acceptor was uphill.

Effects of Interfacial Energetics, Doping Density, and Light Intensity. Figure 9 has been constructed to depict quantitatively the energetics of the p-InP/CH_3CN interface during these experiments as determined from capacitance measurements. As indicated in the text and in other publications,[13,18,19] appropriate etching procedures for the p-InP electrodes and the presence of a thermal electron acceptor in the solution result in frequency-independent, nonhysteretic M–S plots, indicating that the band edges did not shift during the experimental procedure. Capacitance measurements were well suited for determination of band-edge positions, since these measurements were obtained under experimental conditions identical to those of the RRDE light modulation experiments. Other methods such as photocurrent onset and photopotential measurements are less accurate and require substantially higher photon fluxes.

Ring/disk experiments using DFER$^{+/0}$ as the thermalized carrier revealed a strong dependence of the percent hot photocurrent on the applied potential. Since the band-edge positions remained constant, as illustrated by the M–S plots, a rational explanation for the dependence of production distribution on doping density and applied potential is hot-electron transport across the interface. The proposed mechanism for this process is depicted in Figure 9b and has been called a Type I hot-electron process. Injection of electrons into the electrolyte at energies negative of E_{CB} results from the strong electric field present at the interface, not from excess energy associated with photon absorption (Type II hot carrier). If the photoreduction were occurring through the conduction band edge via a completely thermalized process, one would expect the total photocurrent to increase slightly (due to the wider SCR) as the potential is stepped

(18) Aspnes, D. E.; Studna, A. A. *Appl. Phys. Lett.* **1981**, *39* (4), 316.
(19) Tuppen, C. G.; Conen, B. H. *J. Cryst. Growth* **1987**, *80*, 459.

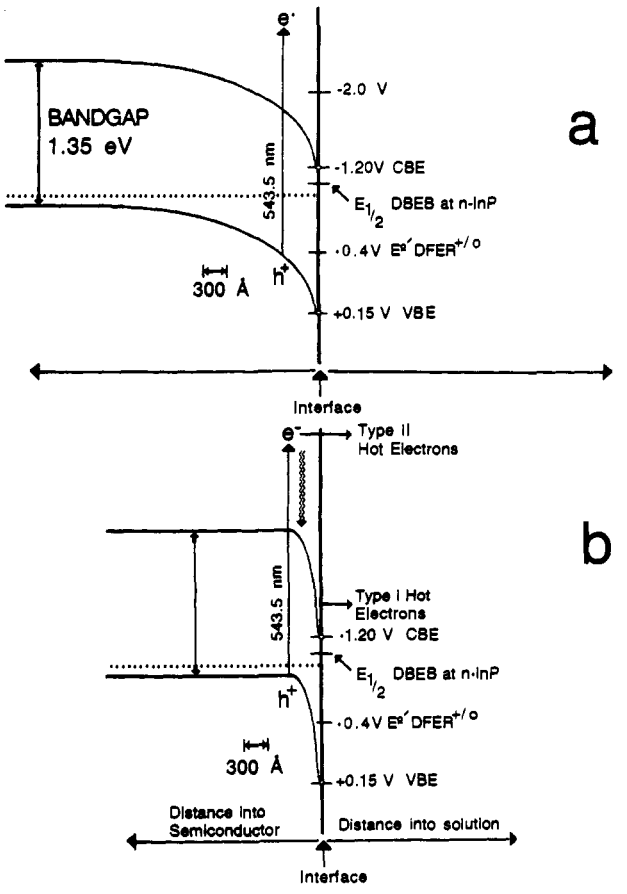

Figure 9. Quantitative semiconductor/solution diagram depicting the energetic conditions of a low-doped (a) and high-doped (b) semiconductor electrolyte under 1.0 V of band bending. The width of the space charge region and the energy of the photogenerated electron are proportionally scaled in the diagram. The region where the electron/hole pair is created represents the depth at which 97% of the 543.5-nm photons are absorbed.

negative, but the product distribution should remain unchanged. Instead, the Type I hot-electron model predicts that, as band bending increases, the energy states residing very near the conduction band edge become quantized and discrete. This potential dependence effect was observed in all experiments where hot carriers were detected.

As the data in Tables I and II indicate, a significant difference in the product distribution was observed between the high- and low-doped electrodes. Under identical experimental conditions, the high-doped electrode exhibited a higher fraction of DBEB reduction in all instances. These observations are consistent with a Type I hot-electron mechanism; however, one might argue that differences in the position of E_{CB} for individual electrodes were responsible for this effect. For the experiments at higher light intensities (Table I entries a and b, Table II entry d), E_{CB} for the low-doped electrode was actually negative of the values measured for the high-doped electrodes. Therefore, if the doping-density dependence of the product distribution were due to the position of E_{CB}, greater amounts of DBEB reduction would have been observed for low-doped electrodes. At the lower light intensity (Table I entry c and Table II entry e), a direct comparison of the high- and low-doped electrodes is impossible due to the large difference in E_{CB}.

Figure 9 quantitatively depicts the differences between the depletion depth and electric field present at the interface for high- and low-doped electrodes. Due to these differences, the time required for a photogenerated electron to traverse the width of the space charge region in a high-doped electrode is approximately 2 orders of magnitude shorter relative to that for a low-doped electrode. Using longitudinal reflective electro-optic sampling techniques, Miller et al. have shown that the charge carrier transport across the space charge region of n-doped (100) orientated GaAs/oxide interfaces occurs in much less than 500 fs.[20] Time scales for electrons reaching the surface of highly biased InP electrodes are likely to be equally short. In order for hot-electron transfer to occur, the electrons must react before they thermalize to the band edge. Thermalization of hot carriers occurs through inelastic collisions between charge carriers and phonons. For electrons in III–V semiconductors such as InP only polar, longitudinal optical (LO) phonon interactions dominate the cooling of electrons.[21] Recent studies on InP and GaAs of carrier thermalization dynamics using subpicosecond luminescence spectroscopy have found that the electron density between 100 and 200 mV above the bottom of the conduction band peaks about 2–10 ps after the excitation pulse.[22] A hot-carrier reaction requires that the electron-transfer time from semiconductor to solution must be on a comparable time scale with thermalization. In a recent review, Lewis[4] concluded that thermalization times would have to be longer than 1 ns in order for reaction with outer-sphere redox couples at concentrations <10 mM to be significant. This analysis is based on the assumption that intrinsic electron-transfer rate constants for hot electrons are identical to those for thermalized electrons. One possibility that would allow our results to be consistent with the theoretical model is that the high kinetic energy associated with photogenerated electrons in high-doped p-InP results in unusually large interfacial electron-transfer rate constants. Of course, a second possibility is that the DBEB molecules are adsorbed; however, this same rationalization must be used to explain the similar results with Cu(trans-diene). Voltammetric experiments at platinum and n-InP revealed no prewaves or anomalous behavior which are indicative of adsorption, see Figures 1, 2, and 3. Adsorption on an electrode surface can inhibit an electrode reaction by formation of an impervious layer that blocks a portion of the electrode surface, or it can accelerate the electrode reaction through electrocatalytic effects. Photocurrents at p-InP as well as steady-state currents at platinum and n-InP all reveal stable current vs time profiles, see Figure 4. In addition, since styrene is a product of the DBEB reduction, one can conclude that the polymerization of styrene is not occurring on the surface of the electrode. Furthermore, capacitance measurements gave no indication that neither DBEB nor Cu(II,I)(trans-diene)(2+/1+) is adsorbed at InP,[9] see Figure 8.

When the illumination source was attenuated, the distribution of photoreduction products changed considerably for the high-doped p-InP electrodes while the conduction band edge position remained unchanged. The percentage of photocurrent attributable to DBEB reduction decreased roughly by a factor of 3, independent of applied potential, even though the quantum efficiency remained unchanged. This result supports a hot-electron-transfer process. It is possible that the mechanism for hot-electron transfer is facilitated at higher photon fluxes due to a phenomenon known as a "hot-phonon bottleneck". This process can be described as a nonequilibrium phonon population induced by high concentrations of photoexcited charge carriers.[23] Reabsorption of the hot phonons by the photoexcited electrons will increase the thermalization times, since the re-absorption of hot phonons will tend to reheat the electron population.

The low-doped electrode showed similar effects at lower light intensities; however, the band-edge positions were dissimilar in these experiments (shifted by >250 mV). The most likely explanation for this large shift in E_{FB} is that the low-doped electrode was re-etched between experiments d and e, which were performed on different days. The high/low light intensity

(20) Min, L.; Miller, R. J. D. *Appl. Phys. Lett.* **1990**, *56*, 524.
(21) Shah, J. *Solid-State Electron.* **1989**, *32*, 1051.
(22) Lugli, P.; Gossard, A. C.; Shah, J.; Deveaud, B.; Damen, T. C.; Tsang, W. T. *Phys. Rev. Lett.* **1987**, *59*, 2222.
(23) (a) Lugli, P.; Goodnick, S. M. *Phys. Rev. Lett.* **1987**, *59*, 716. (b) Joshi, R. P.; Ferry, D. K. *Phys. Rev. B* **1989**, *39*, 1180. (c) Shum, K.; Junnarkar, M. R.; Chao, H. S.; Alfano, R. R.; Morkoe, H. *Phys. Rev. B* **1988**, *37*, 8923.

experiments with the high-doped electrode (b and c) were performed on the same day without re-etching.

As mentioned earlier, differences associated with the surfaces of individual p-InP electrodes have significant effects on the photoelectrochemical behavior. These effects include minor changes in band-edge positions and different percentages of hot photocurrent. For all of the high-doped electrodes DBEB reduction was never eliminated, only diminished. Nevertheless, this etching-induced variability presently makes it difficult to obtain mechanistically important information, such as the reaction orders for DBEB and $DFER^+$. Present research activities involve use of surface analysis to understand the more subtle effects of etching on photoelectrochemical behavior.

Acknowledgment. The authors thank Dr. John Turner of NREL for providing us with the computer software used in the Mott–Schottky capacitance analysis. Discussions with A. J. Nozik (NREL), N. S. Lewis (Caltech), and R. J. D. Miller (University of Rochester are also a pleasure to acknowledge. This work was support by the Department of Energy (Division of Chemical Sciences) Contract # DE-FG02-84ER13247.